Chapter 2

New Approaches to the Friction Stir Welding of Aluminum Alloys

Marcello Cabibbo, Archimede Forcellese and Michela Simoncini

Additional information is available at the end of the chapter

http://dx.doi.org/10.5772/64523

Abstract

Friction stir welding (FSW) is a technique able to guarantee welding advantages such as the easy control of tool design, rotation speed, and translation speed. This is also a reason for a continuous research activity to optimize the effect of the different welding parameters and tool-metal setups. In this contribution, two innovative welding methodologies are presented and discussed. A first new FSW configuration was defined as double-side friction stir welding (DS-FSW). In the DS-FSW, the welding is performed on both sheet surfaces, that is, the first welding is followed by a second one performed on the opposite sheet surface. In this chapter, the effect of the welding parameters, tool configuration and sheet positioning on the yield, ultimate strength, and ductility of an aluminum plate, its microstructure and its post-welding formability are discussed. A second new FSW configuration consists of a pin rotation around its centerline welding direction by 0.5 and 1.0 mm. This was defined by authors as RT-type configuration and it is characterized by a welding motion of the pin tool obtained by the combination of two different movements occurring simultaneously.

Keywords: FSW, tensile strength, ductility, LDH, FLC, hardness

1. Introduction

The continuing scientific and technological attention to reduce vehicle weight and emissions resulted in a diffuse use of Al alloys as a substituting metal with respect to steel, in many applications that were formerly dominated by steel. This change of technology metallic material has strongly promoted tailor-welded blanks new solutions especially in the vehicle applica-

tions [1, 2]. Laser-beam welding and friction-stir welding (FSW) are currently considered to be the most prospective welding processes.

Anyhow, the common difficulties involved in laser welding of aluminum alloys include porosity, hot cracking, poor coupling (due to the high reflectivity of the metal), and degradation of the material properties in the heat-affected zone (HAZ) [3–5]. Despite several advantages offered by laser beam welding applied to aluminum alloys, this welding technology usually suffers from seam imperfections such as notches, which reduce the mechanical properties of the joint [5]. In order to overcome such drawbacks, the friction stir welding (FSW) has strong potentials against the laser beam welding, as it is a solid-state welding technology [6, 7]. In this sense, FSW is surely considered to be the most significant development in the metal joining techniques over the past two-to-three decades. The nonwelded nugget zone (NZ) makes this welding technology an energy-effective one. It is also an environmentally friend and a versatility welding technique often considered as a "green" technology. In fact, compared to the fusion welding processes, FSW consumes less energy with very low fraction of wasted material and a drastic reduction of dangerous fumes production [3–7].

Moreover, FSW produces a high-quality joint, compared to other conventional fusion welding processes. It is also a welding process particularly suited for joining nonmetal materials to metals, especially in those cases where it is not possible by using conventional fusion methods [8, 9]. Its key factors and main properties consist of the welding nature of the FSW metals. The weld zone undergoes a solid-state process promoted by the frictional heat between a rotating tool and the welding metal. The plasticized zone, induced in the material by the rotating tool, is further extruded from the leading side (advancing side, AS) to the trailing side (retreating side, RS) of the tool during its steady translation along the joint line [10]. Neither filler material nor shielding gas is required. The temperature involved is typically some 50–100°C below the metal melting point, and thus there is no volume change during joining. Moreover, it is generally agreed that FSW, compared to the fusion welding techniques, induces rather low residual stresses after welding. This also implies process-reduced manufacturing costs [11].

As for the welded alloy mechanical properties acquired after the welding process, the FSW generally guarantees better tensile, bend, and fatigue properties than fusion welds. Taking advantages of these positive factors, this process has already been applied to a great variety of aluminum alloys, other than many other metallic materials. In the case of the aluminum alloys, the FSW technique has found many applications, such as external fuel tank of rockets, stock of railways, bridges [12, 13], to cite but few. Other interesting applications of FSW in the aerospace industry include fuselage, structural parts, cryogenic tanks, etc. [10]. Other interesting applications also include the marine applications (like offshore industry) [10, 14].

The microstructure modifications occurring at the central FSW zone (i.e., NZ) most usually consists of dynamic recrystallization resulting in the formation of fine equiaxed grains [8, 16]. This recrystallized zone can slightly reduce the welded alloy mechanical properties. For this reason, an accurate choice of the process parameters (rotational speed, welding speed, tilt angle, and sinking) and of the tool geometry (pin and shoulder geometry and size) is required. In fact, by increasing the pin rotational speed or by decreasing the welding line progression, the alloy mechanical properties can usually be optimized [15, 16].

One of the main welding defects, from which FSW is likely to be affected, is the oxide layer formation on the butt surface ("kissing-bond" phenomenon). The kissing-bond generally means a partial remnant of the unwelded butt surface below the stir zone. Its formation is mainly attributed to insufficient plunging of the welding tool during FSW [17], and it is usually responsible of the formation of small geometric discontinuities into the NZ [18].

2. Novel approach to the FSW process

In this context, the present contribution shows the effect of the process parameters, tool geometry, and size on macromechanical and micromechanical properties of FSWed joints by using a conventional pin and a nonconventional pinless tool configuration. The potential advantages offered by the pinless tool configuration can be fully exploited only as thin sheets are welded since, as the thickness increases, the shoulder influence becomes ever more localized to the top sheet surface.

A new FSW approach is here presented. This was developed to promote a better joint formability and it consists of carrying out the FSW process on both the sheet surfaces. In this process, the first welding operation is followed by a second welding performed at the plate opposite surface. Such an innovative methodology has been defined by these authors as double-side friction stir welding (DS-FSW) [19, 20]. This new FSW methodology has proven to be able to seal the geometric discontinuities, possibly produced by the first welding process, by means of the second welding operation performed at the opposite surface at the same experimental conditions. In addition, this new approach allows more uniform hardness values across the NZ. Moreover, the recrystallized grain size across the NZ is more homogeneous with respect to the surrounding FSW zones, compared to the conventional FSW, as shown by Cabibbo et al. [20]. Such improvement in the joint quality is very attractive, especially in those cases where the joint materials are meant to be subjected to post-welding forming operations. The hardness and local Young's modulus, determined by nanoindentation, were used to probe the overall weld joint strength. Nanoindentation profiles are also used to correlate the sub-micrometer hardness values to the corresponding FSW microstructure, and finally to properly correlate the welded plate formability with the welded sheet microstructure and micromechanical response.

A further novel approach to the FSW process (defined by authors as RT-type [21]) is also reported. This new configuration consists of a combination of different plate-to-pin motions. In one configuration, the pin axial spin rotation is set perpendicularly to the sheet blanks travelling along the welding line, with a lateral rotation radius $R = 0$, 0.5 and 1 mm. In a second configuration, the pin translation along the welding plate is set parallel to the welding line. Both these new welding approaches were compared with the conventional FSW practice, in which the welding motion occurs linearly along the welding line (and this conventional configuration is here defined by authors as T-type). With this respect, the two here proposed new configurations were also characterized using tools with different pin heights. These involved different sinking values during FSW. The study of the new setup also includes plate

heat treatments, such annealing, prior and after the FSW. The effect of the radius R, pin height, and annealing treatment on microstructure, micromechanical and macromechanical properties is here discussed in order to define the process condition and the temper state that allows to obtain defect-free joints, without the occurrence of the oxide defects of kissing-bonds, and faint zigzag line pattern in the NZ.

3. Description of the new FSW process setups

FSW experiments were carried out using a computer numerical control (CNC) machining center.

3.1. DS-FSW method

As for the DS-FSW method, a conical pin tool geometry (H13 steel of HRC = 52), with a shoulder diameter equal to 12 mm and cone base diameter and height of the pin of 3.5 and 1.7 mm, respectively, with a pin angle of 30°. A 19-mm-diameter rotating tool was used. All the welding experiments were carried out with a nutting angle equal to 2°.

In DS-FSW, the first welding is followed by a second one, performed at the opposite surface, with respect to the first welding operation. Two different sheet positions, with respect to the welding tool, were investigated and are here presented:

(1) AS-AS, in which the sheet is placed in the AS, at the first FSW operation, and it is maintained in the same side also at the second FSW passage at the opposite surface;

(2) AS-RS, in which the sheet, placed in the AS at the first FSW, to be reversed, in the RS, at the second FSW passage at the opposite surface.

In both configurations, the effect of tool configurations on the quality of the DS-FSW joints was also analyzed.

In **Table 1** are reported the different tool configurations and sheet positions used in the DS-FSW. The used blanks were 180 mm in length, 85 mm in width, and 2 mm in thickness. The FSW was performed by fixing the welding line perpendicular to the rolling direction.

Sheet position	Tool configuration for the first pass – and second pass
AS-AS	Pin-pin
AS-RS	Pin-pin
AS-AS	Pin-pinless
AS-RS	Pin-pinless
AS-AS	Pinless-pinless
AS-RS	Pinless-pinless

Table 1. DS-FSW configurations (in terms of tool used and sheet arrangement).

http://dx.doi.org/10.5772/64523

The effect of the process parameters on the conventional and the DS-FSW was inferred using homologous rotational speed values (ω), which ranged 1200–2500 rpm, and same welding speed (v), equals to 60 and 100 mm/min. The conventional FSW was carried out using a tool sinking of 0.2 mm, while the DS-FSW was performed with a sinking of 0.15 mm in the first pass and 0.05 mm in the opposite surface. These welding parameters were set on the basis of the results obtained by preliminary tests, carried out using different tool sinking values, showed the need to perform the second pass with a sinking lower than that of the first one in order to prevent the occurrence of fracture.

In **Table 1** DS-FSW AS-AS pin-pin consists of maintaining fixed the AS and RS for both welding procedures; AS-RS pin-pin consists of reversing the AS into RS, from the first to the second welding procedure.

The third and fourth configuration differs from the first two only in the absence of the pin during the second welding process. In the last two (AS-AS, and AS-RS pinless-pinless), the welding process was performed with no pin in both processes. **Figure 1** shows a schematic representation of the three DS-FSW configurations used here.

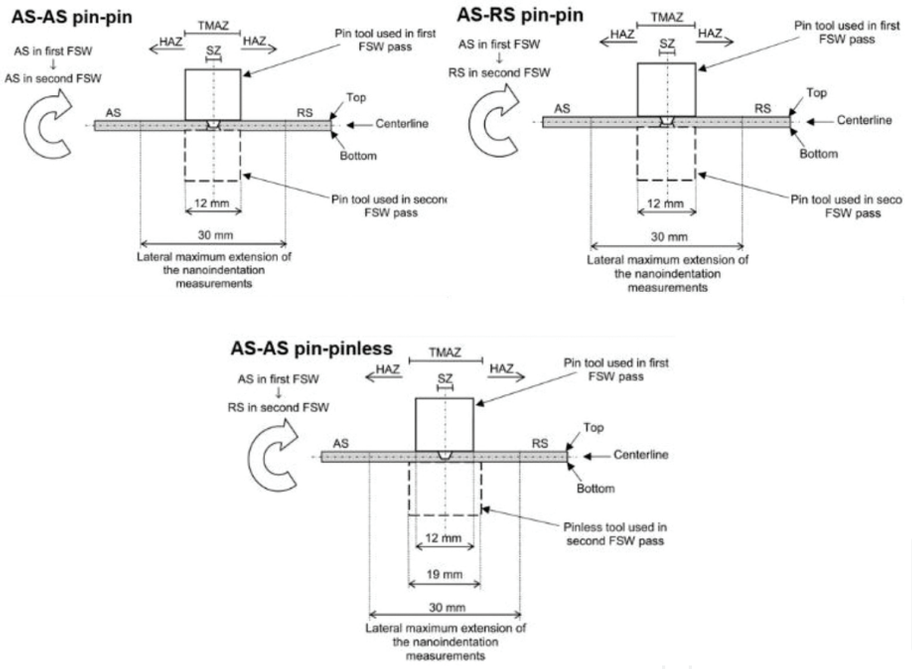

Figure 1. Representation of the three DS-FSW configurations: AS-AS pin-pin (left side); AS-RS pin-pin (center); AS-AS pin-pinless (right side).

3.2. Pin rotation deviation from centerline (RT-FSW) method

As for the pin rotation configuration method, the innovative approach to the FSW process was defined by authors as RT-type. For this purpose, a conical pin tools in H13 steel (HRC = 52) with a 2.3 mm pin height, 3.9 mm in diameter at the shoulder, a 30° pin angle, and a shoulder diameter of 15 mm (applying a vertical force of 1.7 kN) was used (**Figure 2**).

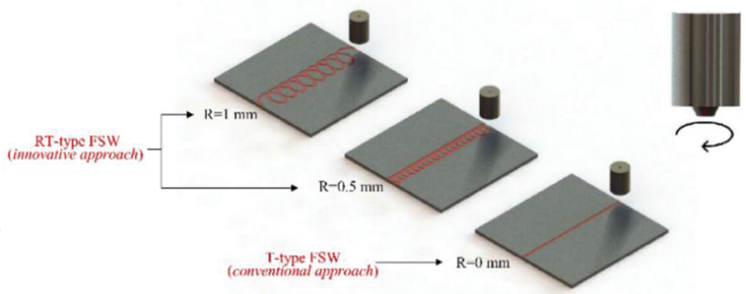

Figure 2. Comparison between conventional (R-type) and T-type FSW configurations.

The welding motion combines two different plate-to-pin mutual motion setups:

(1) a pin axial spin rotation sets perpendicular to the sheet blanks, changing the rotation along the plate centerline by a radius equal to R (=0, corresponding to the conventional FSW, 0.5, and 1 mm);

(2) a pin translation along a direction parallel to the welding centerline line.

The RT-type FSW innovative approach was compared with the conventional T-type (linear welding motion, i.e., for $R = 0$). In both the RT-type and T-type FSW processes, the stirring action was exerted by the pin tool rotation around its axis; the pin tilt angle was set at 2°, with respect to the normal direction to the plate surface. The RT-type and T-type FSW were performed using a pin rotational speed, $\omega = 2000$ rpm, and a transverse speed, $v = 30$ mm/min. All experiments were carried out with a tool plunging speed of 1.5 mm/min. The above reported setting parameters were chosen by an optimization FSW processing study reported in [22], where the effect of the welding parameters and tool configuration on micromechanical and macromechanical properties of FSW joints in AA5754 sheets were investigated. The AA5754 was subjected to an annealing treatment at 415°C/3 h, both prior (AA5754-O), and after (post-weld annealing, PWA), followed by furnace cooling.

4. The material

In both the cases, aluminum alloys were tested. In the first methodology, a heat-treatable AA6000-series alloy (AA6082) was used; whereas in the second methodology, a nonheat-treatable AA5000-series alloy (AA5754) was welded.

The AA5000-series alloys, such as the AA5754, are widely used in automotive, aerospace, marine, and military applications. They are characterized by a good strength-to-weight ratio, an appropriate weldability, and a good corrosion resistance. This class of aluminum alloy is difficult to join by conventional fusion welding techniques. This is mainly due to a dendritic structure, which typically forms in the melted zone and it seriously weakens the mechanical properties of the joint AA5000 series alloys. In this context, FSW has emerged as a promising solid-state process with the successfully overcome the fusion welding problems, making the welding process of AA5000 series alloys a sound one [23]. FSW of AA5754 is thus a promising

technique to obtain sound welded joints, either in similar [24, 25] and dissimilar [26, 27] welding combinations (using AA5757 or AA5083).

In the present case, the AA5754 sheets were produced by twin roll continuous casting followed by cold rolling to give a H111 (EN485) metallurgical initial status and a thickness of 2.5 mm.

The AA6000-series are widely used because of their good weldability, corrosion resistance, and immunity to stress-corrosion cracking. These are known to be among the most used aluminum alloys for extruded components [28]. In fact, AA6082 (Al-Mg-Si) typical application include aeronautics, automotive, and recreation industries. In the present case, cold-rolled sheets of AA6082 were used to show the soundness of the DS-FSW.

5. Experimental findings and evidence for sound and better FSW joints

5.1. The DS-FSW method

There is a strong need for an improvement in ductility and formability of FSWed joints. Some previous studies reported significant mechanical improvements by carrying out multipass [29], double lap [30], reverse dual rotation [31] FSW, and FS spot welding [32]. With this respect, the DS-FSW showed better strength, elongation, and formability of FSWed aluminum joints. The DS-FSW was proven to induce the serration of the geometric discontinuities, thus promoting a significant microstructure homogeneity at the NZ.

5.1.1. Mechanical properties

Figure 3 shows typical nominal stress versus nominal strain curves of FSWed joints in AA6082 obtained under different values of the rotational speed and welding speed. The joints ductility is shown to be lower in the NZ, with respect to the base metal (BM), irrespective of the welding parameters and process methodology [22]. In general, in terms of both the ultimate values of tensile strength and elongation, the conventional FSWed joints show a tensile behavior better than the one exhibited by the DS-FSWed joints. Actually, the conventional FSW process requires a high sinking value in order to generate the frictional heating allowing the material flow necessary to obtain sound joints, according to Mishra and Ma [7]. Thus, in the first pass, by using the same tool sinking as of conventional FSW produces a step in the blank surface that acts as a notch during the second pass. Therefore, the tool sinking value imposed in the second pass had to be further decreased in order to reduce the formation of surface defects. The pinless-pinless configuration has provided the worst tensile properties. In particular, the AS-AS configuration showed low mechanical properties of the joint, while the AS-RS configuration did not reach a sound weldment.

The mechanical behavior is strongly improved when welding is performed using the pin-pinless configuration. In this case, ductility levels similar to the ones showed by the conventional FSWed samples were obtained. In this case, the tensile fracture occurred at the HAZ, in the RS zone. The tensile properties of the joints are slightly affected by the rotational and welding speeds. This is not the case in the DS-FSW pinless-pinless tool configuration, which

exhibits ultimate tensile strength (UTS) and UE values strongly dependent on the process parameters (**Figure 3**). As a matter of fact, as the thickness increases, the shoulder influence becomes ever more localized near the top surface of the sheet and, consequently, the stirring action becomes less and less effective. With this respect, in published work by these authors, the FSW capability to obtain sound joints in 1- and 1.5-mm-thick sheets using a pinless tool was widely documented [20, 22, 33].

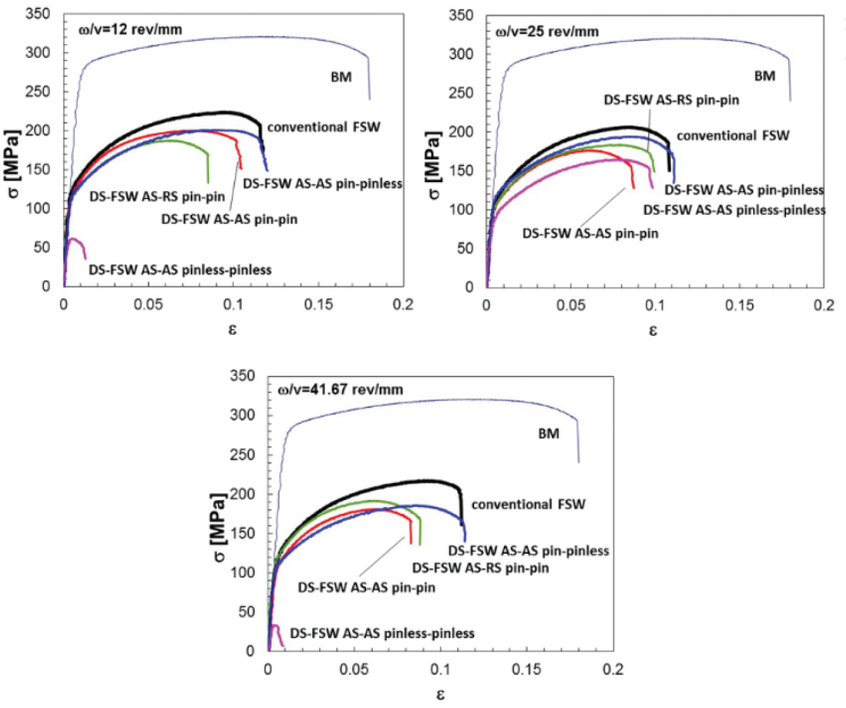

Figure 3. Tensile stress-strain curves of the DS-FSW, with different welding parameters and tool configurations.

5.1.2. Post-welding formability

In comparison with conventional fusion welding techniques, one of the most important advantages offered by FSW is the relatively high post-welding formability. In this sense, the conventional FSW and the DS-FSW formability, obtained under the same process conditions, was detected. For this purpose, limit dome height (LDH) analyses were carried out. These values represent the punch stroke at the peak of the load versus the stroke curves. It actually represents the dome height of the deformed samples at the onset of necking, and the results are reported in the plot of **Figure 4**. These data agree with the joint ductility obtained by tensile tests (**Figure 3**). The LDH values were lower than those obtained on the BM, no matter what welding methodology was used. Such results reveal that a noticeable formability reduction along the welding zone [18, 20, 22, 33–35]. More specifically, the B arrangement leads to a LDH value lower than the T arrangement (as reported by the letter B and T in **Figure 4**, and according to the configuration reported in **Figure 5**).

http://dx.doi.org/10.5772/64523

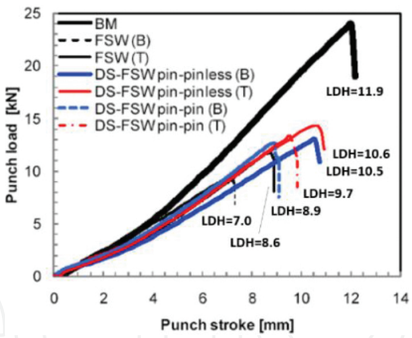

Figure 4. Hemispherical punch test for different testing conditions (LDH is the Limit Dome Height).

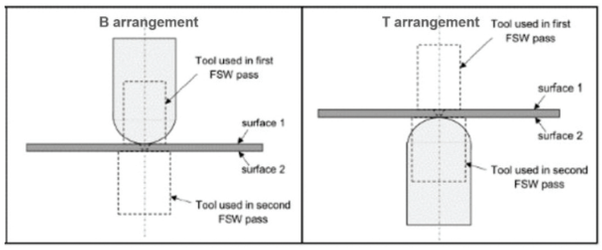

Figure 5. Hemispherical punch test configurations. In the B arrangement, surface 1 is in contact with the punch; in the T arrangement surface 1 is opposite.

In the B arrangement, the local stress field intensity rise, caused by the notch, is responsible of the FSW sample failure at the geometric discontinuity. In the T arrangement, that is, FSWed blank having the notch in contact with the punch, the failure of the deformed joint occurs at the step produced by the sinking action applied by the shoulder [19]. This is mainly due to the biaxial tensile stress state to which the notch is subjected. This appeared to be less severe in the T arrangements, with respect to that in the B arrangement.

The DS-FSW joints showed LDH values higher than those measured on the conventional FSWed joints. This is likely to be attributed to the beneficial effect of the second pass of the DS-FSW. This second welding induces a dual beneficial effect: it allows both the closure of the geometric discontinuity, and the reduction in the height of the step produced by the first welding on the opposite plate surface. Furthermore, the DS-FSW is characterized by more uniform recrystallized grains across the NZ, and also partially across the thermo-mechanical affected zone (TMAZ), than in the case of the conventional FSW [19]. Finally, the joints obtained using the pin-pinless tool configuration lead to LDH values higher than the ones obtained by using the pin-pin configuration, irrespective of the sheets arrangement. Thus, in the pin-pinless configuration, the LDH value was only ~12% lower than that of the BM. This result appears to be virtually independent of the sheet arrangement. On the other hand, in the pin-pin tool configuration, the LDH reaches values of ~19 and 25% lower than that of BM in the T and B arrangements, respectively (**Figure 4**).

A more accurate evaluation of formability is obtained by means of the forming limit curves (FLCs). This is obtained by plotting the major strain versus minor strain data (**Figure 6**). It

resulted that the formability of the BM is always higher than that of the welded joints. In the stretching side of the FLD, for a given minor strain, the major strain measured on the DS-FSWed joints appeared systematically higher than that provided by the conventional FSWed ones. This result agrees with the behavior exhibited by the LDH (**Figure 4**). The higher vertical position of the FLCs confirms that formability is strongly improved when the DS-FSW technique is used. The comparison among the different FLCs obtained in the DS-FSW, using both the pin-pinless and the pin-pin configurations, shows that the FLCs are scarcely affected by the tool configuration used in the second pass. Finally, the B arrangement is characterized by the lowest major strain values, and this agrees with the LDH results shown in **Figure 4**. This differentiation tends to vanish when DS-FSW is used. It is noteworthy to observe that the process methodology and sample arrangement also affect the extension of the FLCs. In fact, **Figure 6** shows FLCs smaller extension in the welded joints, compared to the BM. Such behavior is almost negligible in the drawing zone of the FLD. This becomes significant in the stretching region, as confirmed by LDH values shown in **Figure 6**.

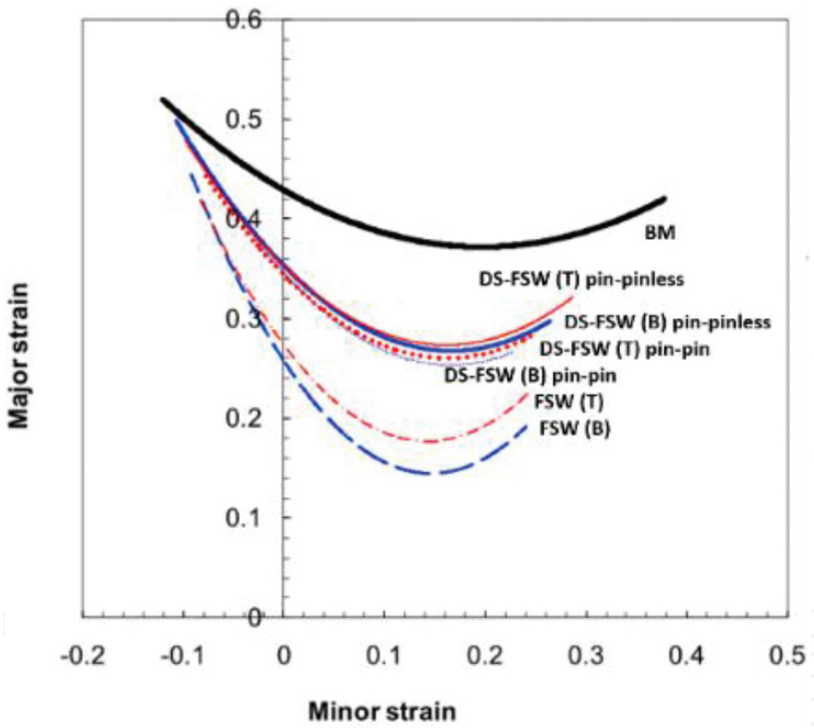

Figure 6. Forming limit curves (FLC) obtained using different welding processes and sample arrangements.

Figures 7 and **8** show the nanoindentation experimental results, in terms of harness and Young's modulus. The main difference between the pin and the pinless FSW consists of the low hardness (H) and elastic modulus (E_r) values obtained at the TMAZ. In the conventional pin FSW, low H and E_r are in the retreating TMAZ, whereas in the pinless FSW, both the advancing and the retreating TMAZ experienced such low H and E_r values. In both the cases, these lower values accounted for a drastic hardness reduction, being three times less, and an elastic modulus reduction of almost ten times, with respect to the BM values.

http://dx.doi.org/10.5772/64523

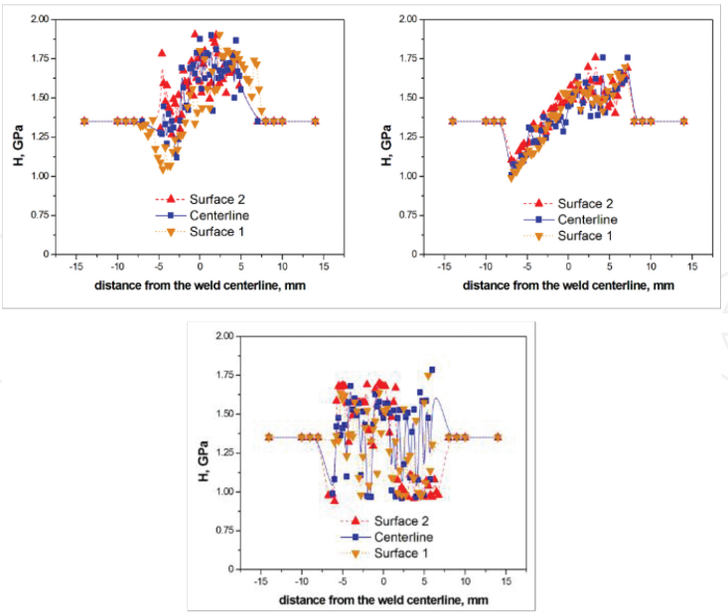

Figure 7. Nanoindentation hardness profiles for the different configurations used.

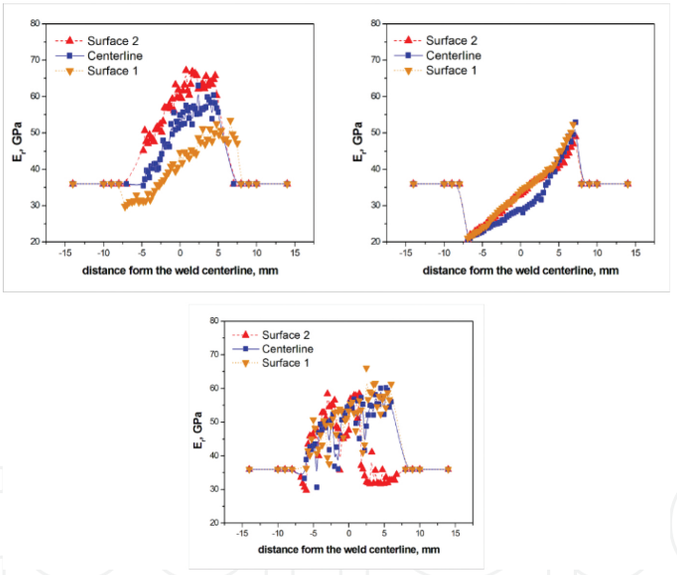

Figure 8. Nanoindentation Young's modulus profiles for the different configurations used.

Moreover, in both the pin and pinless conventional FSW, the lower H and E_r values, recorded at the surface in contact with the shoulder, also pertain to the outer part of the SZ. On the contrary, in both pin and pinless FSW, the profile along the centerline of the sheet section did not show any reduction of H and E_r across the NZ, TMAZ, and HAZ. The hardness, at the section centerline of the NZ, is constantly higher than the BM, with values that peak at 2.05 GPa. In particular, the two AS-TAMZ and RS-TMAZ showed values ranging 1.40–1.55 GPa, while the hardness in the NZ ranged from 1.65 to 2.05. Along the centerline of the pinless FSWed

section, the hardness profile appeared considerably more uniform than the one obtained in the pin FSW. In the former case, the hardness ranged from 1.75 to 2.10 GPa, across the characteristic regions of the FSW joint.

Uniform H and E_r values were obtained across the welded zone in all the three DS-FSW configurations. This was not the case in the two conventional, where hardness appeared far from being uniform across the FSW joint regions. In particular, in the pin-pin AS-AS DS-FSW, the hardness decreased in the TMAZ AS, while the rest of the welded zone (i.e., NZ and RS-TMAZ) showed hardness values significantly higher than the ones of the BM. This trend was common to all the three profiles (upper surface, centerline, lower surface). The elastic modulus increased up to 50%, in the NZ. The top values were reached in the surface where the second FSW took place (Surface 2). Quite similar hardness trends were found in the pin-pin AS-RS DS-FSW. In particular, in the TMAZ RS (at the second welding), the elastic modulus steadily increased from values of almost half respect the BM, to reach values of some 30–35% higher than those of BM, in the TMAZ AS. Finally, in the pin-pinless AS-AS DS-FSW, H and E_r profiles, taken along the upper-surface, centerline, and lower-surface, were essentially similar to those observed in the pin-pin AS-AS DS-FSW. The only significant difference was the rather fuzzy and wavy hardness trend obtained in this case, at the AS-TMAZ, SZ, and RS-TMAZ.

The better formability of the DS-FSW, with respect to the conventional FSW, is most likely related to the local elastic modulus uniformity (i.e., the reduced Young's modulus) across the weld, and to the less dramatic hardness variation, from top to bottom of the sheet section.

5.1.3. Microstructure of joints

Table 2 reports the mean grain size as a function of welding methodology and tool configuration, measured at different zones of the welded joints. The considerably small grain size in the SZ, combined with the equiaxed grain shape, implies the occurrence of dynamic recrystallization because of the very high levels of deformation and temperature reached in such zone during FSW [35].

FSW configuration	Mean grain size, μm				
	AS/TMAZ	Surface 1/SZ	Middle/SZ	Surface 2/SZ	RS/TMAZ
Conventional	14 ± 2	7.8 ± 0.3	7.6 ± 0.3	6.9 ± 0.3	14 ± 2
DS-FSW pin-pin	12 ± 2	6.3 ± 0.2	6.2 ± 0.2	6.4 ± 0.2	13 ± 2
DS-FSW pin-pinless	12 ± 2	5.7 ± 0.2	5.7 ± 0.2	5.8 ± 0.2	13 ± 2

Table 2. AA6082 DS-FSW mean grain size; the BM SZ had a mean grain size of 20 ± 2 μm.

In the conventional FSW, the grain size within the SZ tended to increase near the top of the weld zone, and this is chiefly due to the temperature variation within the weld zone [36]. In all the three DS-FSW configurations described here, the observed grain size uniformity and

morphology across the SZ, from surface to surface, greatly favored the soundness and better post-welding response of the welded Al-sheets.

5.2. The friction stir welding method by pin rotation deviation from centerline: RT-FSW

Rotation of the pin from its centerline progression, during the FSW process, is intended as a further possible improvement in the welded soundness of aluminum plates.

5.2.1. Mechanical properties

Figure 9 shows typical stress-strain tensile curves of both as-received and FSW AA5754 sheets. The ultimate tensile strength (UTS) and plastic elongation (El) values are reported in **Figure 10**. The mechanical response is quite different as the pin moves in RT-type configuration with R = 0.5 mm. In this case, the UTS reduction respect to the unwelded sheet was 25%, that is double that for R = 0 mm (T-type FSW). At R = 0.5 mm, ductility (El) was 78%, respect to the unwelded sheet, and thus it was three times lower with respect to the ductility obtained at R = 0 mm (in the T-type FSW). UTS reduction, compared to the unwelded sheet, accounted for 20 and 22%, respectively; the ductility reduction was 48 and 74%, accordingly.

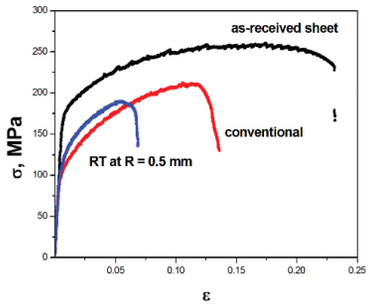

Figure 9. Tensile stress-strain curves for RT-FSW at R = 0 (conventional FSW), and 0.5 mm.

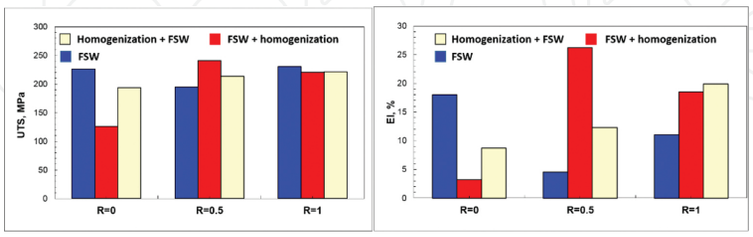

Figure 10. UTS and El of the AA5754 RT-FSW.

The tensile curves, irrespective of the specific FSW setup (T- and RT-type FSW), clearly showed the occurrence of serrated yielding, also termed the Portevin-Le Chatelier (PLC) effect, that is a common phenomenon in 5xxx aluminum alloys [36, 37]. The PLC phenomenon is driven by Mg solute atom cloud formation. This microstructure atomic-level evolution is actually

responsible for the strain rate dependency of the observed serrated yielding phenomenon. The Mg solid solution, induced in the grains of the cold-rolled AA5754 sheets, effectively pins the dislocation sliding motion induced by the tensile test. This, in turns, generates the yielding phenomenon.

5.2.2. Microstructure of the joints at the different pin rotation radii

Figure 11 shows an overview of the FSW plate microstructure, in which the occurrence of a grain dynamic recrystallization process in the NZ is evident.

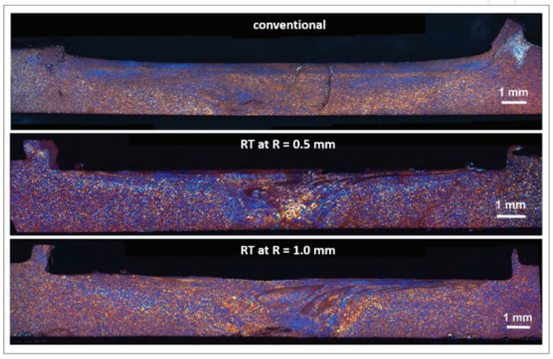

Figure 11. Montage of polarized optical micrographs (POM) RT-FSW at $R = 0$ (conventional FSW), 0.5, and 1 mm.

5.2.3. Microstructure modifications induced by pre- and post-welding annealing

The AA5754 was subjected to an annealing treatment at 415°C/3 h followed by furnace cooling, in one case prior FSW (AA5754-O state), and in another case, after FSW (post-weld annealing: PWA).

The microstructure of the annealed FSW AA5754-O sheets, obtained both under T-type and RT-type FSW configurations, is shown in **Figure 12**. As expected, the base material (BM) is fully recrystallized. It appeared that the equiaxed recrystallized mean grains did not change significantly in the BM, HAZ, and TMAZ, on either AS and RS of joint. This was found irrespective of the pin deviation extent. The NZ-grained structure, in the conventional ($R = 0$), and for 0.5 mm pin rotation deviation, appeared to be mixed, and characterized by the coexistence of fine equiaxed grains and stirred elongated grains (still remaining of the stirring effect induced by the FSW). It is actually a microstructure modification induced by concurring effect driven by the first recrystallization stage (due to the annealing treatment at 415°C/3 h), and by the following mechanical heat flow during the FSW. This latter is known to rise the temperature in the NZ aluminum alloys typically by 350–500°C [20, 27, 37]. The tool shoulder rotation, during welding, induces a large heat transfer and a high strain level at the top surface, which is considerably higher than that induced at the bottom surface. The bottom surface was in contact with a back-plate support, during the welding process. This indeed acted as a heat sink lowering the peak temperature and reducing the time to the peak temperature. Thus, in turns, grain growth in the bottom surface of the NZ was effectively slowed down during the

http://dx.doi.org/10.5772/64523

welding process. The NZ, obtained with R = 1 mm, still presented some oxide layers both in its center and near the TMAZ/NZ boundary.

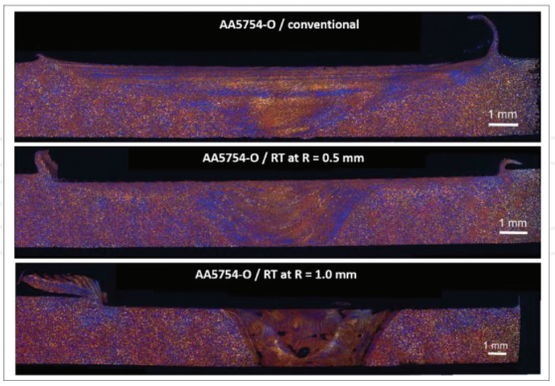

Figure 12. Montage of POM RT-FSW AA5754-O at R = 0 (conventional FSW), 0.5, and 1 mm.

The microstructure of the post-weld annealed (PWA) sheets, for the different rotational radii investigated, is shown in **Figure 13**. For R = 0 mm, fine equiaxed grains characterize the whole extension of the FSW sheet. These equiaxed grains had a mean size substantially same as the ones in the BM, and this was found in the HAZ and the TMAZ of the AS and RS. The only exception consisted in the grain size and morphology in upper welded zone, that is, the surface directly in contact with the shoulder, during the FSW. In this zone, very coarse irregular grains were induced to form by the stirring effect, and by the heat flow introduced in the aluminum plate by the tool shoulder. The depth extension of this coarse-grain region accounted for a minimum of one-third to a maximum of half of the whole sheet thickness. In particular, at R = 0.5 mm, fine recrystallized equiaxed grains characterized the whole extension of the BM, HAZ, and the TMAZ, in both the AS and the RS. More specifically, in this case, the NZ was characterized by the occurrence of very coarse irregular grains, mixed with fine recrystallized grains strips located throughout across the NZ, from the upper to the lower surface. The primary factors leading to the occurrence of abnormal grain growth process, during FSW, are associated with inhomogeneous gran deformation.

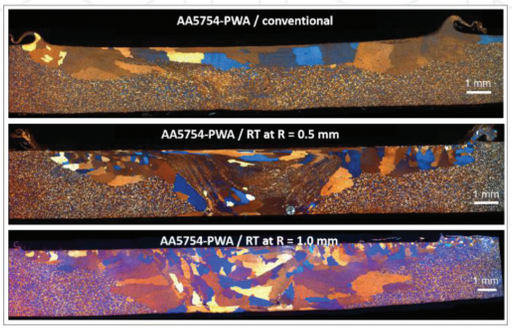

Figure 13. Montage of POM RT-FSW PWA at R = 0 (conventional FSW), 0.5, and 1 mm.

5.2.4. Defect and void formation during FSW

Traces of the presence of oxide layers (the lazy S-lines) are evident in the NZ microstructure (**Figures 12** and **13**). These, actually, follow the location of the fine grain strips. It thus appeared that the fine grains are formed where the oxide layers, the lazy S-line oxides, are present, and were formed at R = 1 mm of RT-type FSW. Thus, it appeared that the fine grain strips, at R = 0.5 mm, are being formed along already existing lazy S-line oxide, which formed during FSW.

5.2.5. Mechanical properties and hardness modifications induced by pre- and post-welding annealing

Typical stress-strain curves are shown in **Figure 14**. It appeared that the closest mechanical response to the unwelded annealed AA5754 sheet is obtained by welding with R = 0.5 mm in the PWA condition, where UTS differed only by 5%, and ductility differed by 30% with respect to the ductility of the unwelded annealed condition. In the other conditions, the UTS remained within a range of 14% of difference, with respect to the annealed sheet, with a ductility reduction ranging from 76 to 30%.

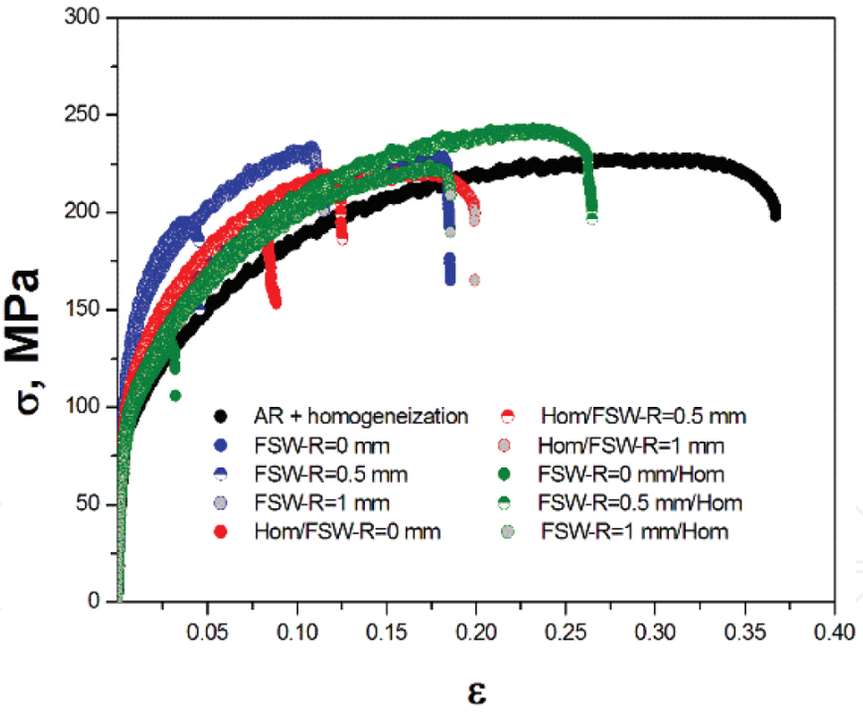

Figure 14. Tensile stress-strain curves for RT-FSW, in the AA5754-O stare and in the PWA condition, at R = 0 (conventional FSW), 0.5, and 1 mm.

Therefore, based on the microstructure evidence, and the obtained hardness and mechanical response, the use of a RT-type welding motion is justified when the plate is homogenized prior, or, even better, after FSW. Conversely, there is no need to deviate the pin, from its welding centerline, in the case of non-annealed AA5000 FSW.

http://dx.doi.org/10.5772/64523

6. Concluding remarks

In this contribution, two novel approaches and methodologies of friction stir welding on aluminum alloys were presented. The first approach consists of a double-side FSW (DS-FSW). The second approach is represented by a radial deviation of the rotating pin from its centerline, during FSW (RT-FSW). Both new methods were tested in a conventional pin and nonconventional pinless configuration. Several interesting achievements, from a technological point of view, were obtained and are here summarized.

DS-FSW:

DS-i: the elastic modulus and the hardness showed a larger uniformity across the sheet section, with respect to the FSW;

DS-ii: A better formability of the DS-FSW, compared to the conventional pin and pinless FSW, was obtained;

DS-iii: The DS-FSWed joints are characterized by LDH, and FLC values higher than those measured on conventional FSW.

RT-FSW:

RT-i: The RT setup, for a pin rotation radius of 0.5 mm, induced a low reduction of the mechanical response, compared to the conventional T setup FSW (i.e., with no pin deviation from the welding line). Accordingly, both the microstructure and the hardness profiles of all the characteristic welded zone were quite similar;

RT-ii: The post-weld annealing (PWA) showed the best mechanical response respect to the unwelded annealed AA5754 sheet. The best experimental setups were obtained setting a pin rotation radius R = 0.5 mm. In this configuration, UTS was ▪ 15% higher, and a ductility reduction of up to 30%, respect to the unwelded annealed sheet. In this condition, the microstructure of the NZ appeared to be characterized by very coarse grains. These coarse grains were generated by geometric dynamic recrystallization (GDR), which is induced by the combined effect of shoulder pressure (heat input), and post-welding annealing (PWA) thermal energy.

Author details

Marcello Cabibbo[1*], Archimede Forcellese[1] and Michela Simoncini[2]

*Address all correspondence to: m.cabibbo@univpm.it

1 DIISM – Department of Industrial Engineering and Mathematics, Marche Polytechnic University, Ancona, Italy

2 Università degli Studi e-Campus, Novedrate, Italy

References

[1] Davies RW, Grant GJ, Oliver HE, Khaleel MA, Smith MT. Forming-limit diagrams of aluminum tailor-welded blank weld material. Metall. Mater. Trans. A. 2001;32:275-283.

[2] Saunders FI, Wagoner RH. Forming of tailor-welded blanks. Metall. Mater. Trans. A. 1996;27:2605-2616.

[3] Merklein M, Johannes M, Lechner M, Kuppert A. A review on tailored blanks-production, applications and evaluation. J. Mater. Process. Tech. 2014;214:151-164.

[4] Sun Z, Ion JC. Laser welding of dissimilar metal combinations. J. Mater. Sci. 1995;30:4205-4214.

[5] Schubert E, Klassen M, Zerner I, Walz C, Sepold G. Light-weight structures produced by laser beam joining for future applications in automobile and aerospace industry. J. Mater. Process. Tech. 2001;115:2-8.

[6] Thomas W, Nicholas ED, Needham JC, Murch MG, Temple-Smith P, Dawes CJ. Friction stir butt welding: International Patent Application PCT/GB92/02203 and GB Patent Application 9125978.8, UK Patent Office, London, December 6, 1991.

[7] Mishra RS, Ma ZY. Friction stir welding and processing. Mater. Sci. Eng. R. 2005;50:1-78.

[8] AU: Data of Ref. [8] was duplicated in Ref. [15]. The latter was deleted, and references and their citations were renumbered accordingly.Su J-Q, Nelson TW, Mishra R, Mahoney M. Microstructural investigation of friction stir welded 7050-T651 aluminium. Acta Mater. 2003;51:713-729.

[9] Seidel TU, Reynolds AP. Visualization of the material flow in AA2195 friction-stir welds using a marker insert technique. Metall. Mater. Trans. A 2001;32:2879-2884.

[10] Nicholas ED, Thomas WM. A review of friction processes for aerospace applications. Int. J. Mater. Prod. Technol. 1998;13:45-54.

[11] Dawes CJ, Thomas WM. Friction stir process welds aluminum alloys. Welding J. 1996;75:41-45.

[12] Heinz B, Skrotzki B. Characterization of a friction-stir-welded aluminum alloy 6013. Metall. Mater. Trans. B 2002;33:489-498.

[13] Mahoney MW, Rhodes CG, Flintoff JG, Spurling RA, Bingel WH. The rate-controlling mechanism in superplasticity. Metall. Mater. Trans. A 1998;29:1955-1964.

[14] Jata KV, Sankaran KK, Ruschau JJ. Friction-stir welding effects on microstructure and fatigue of aluminum alloy 7050-T7451. Metall. Mater. Trans. A 2000;31:2181-2192.

[15] Khorrami MS, Kazeminezhad M, Kokabi AH. Microstructure evolutions after friction stir welding of severely deformed aluminum sheets. Mater. Des. 2012;40:364-372.

[16] Kumbhar NT, Sahoo SK, Samajdar I, Dey GK, Bhanumurthy K.Microstructure and microtextural studies of friction stir welded aluminium alloy 5052. Mater. Des. 2011;32(3):1657-1666.

[17] Oosterkamp A, Oosterkamp LD, Nordeide A. Kissing bond phenomena in solid-state welds of aluminum alloys. Weld. J. 2004;83(8):225s–231s.

[18] Forcellese A, Fratini L, Gabrielli F, et al. Formability of friction stir welded AZ31 magnesium alloy sheets. Mater. Sci. Forum 2010;638–642:1249–1254.

[19] AU: Please provide volume number for Ref. [19].M. Simoncini, M. Cabibbo, A. Forcellese. Development of double-side friction stir welding to improve post-welding formability of joints in AA6082 aluminum alloys. Proc. IMechE Part B: J. Eng. Man. 2015;229:1-11.

[20] M. Cabibbo, A. Forcellese, M. El Mehtedi, M. Simoncini. Double side friction stir welding of AA6082 sheets: microstructure and nanoindentation characterization. Mater. Sci. Eng. A 2014;590:209-217.

[21] M. Cabibbo, A. Forcellese, M. Simoncini, M. Pieralisi, D. Ciccarelli. Effect of welding motion and pre-/post-annealing of friction stir welded AA5754 joints. Mater. Des. 2016;93:146-159.

[22] Simoncini M, Forcellese A. Effect of the welding parameters and tool configuration on micro- and macro-mechanical properties of similar and dissimilar FSWed joints in AA5754 and AZ31 thin sheets. Mater. Des. 2012;41:50-60.

[23] Feistauer EE, Bergmann LA, Barreto LS, dos Santos JF. Mechanical behaviour of dissimilar friction stir welded tailor welded blanks in Al-Mg alloys for marine applications. Mater. Des. 2014;59:323-332.

[24] Movahedi M, Kokabi AH, Seyed Reihani SM, Najafi H, Farzadfar SA, Cheng WJ, Wang CJ. Growth kinetics of Al–Fe intermetallic compounds during annealing treatment of friction stir lap welds. Mater. Charact. 2014;90:121-126.

[25] Costa MI, Verdera D, Costa JD, Leitão C, Rodrigues DM. Influence of pin geometry and process parameters on friction stir lap welding of AA5754-H22 thin sheets. J. Mater. Proc. Technol. 2015;225:385-392.

[26] Kasman Ş, Yenier Z. Analyzing dissimilar friction stir welding of AA5754/AA7075. Int. J. Adv. Manuf. Technol. 2014;70:145-156.

[27] Costa MI, Verdera D, Leitão C, Rodrigues DM. Dissimilar friction stir lap welding of AA 5754-H22/AA 6082-T6 aluminium alloys: Influence of material properties and tool geometry on weld strength. Mater. Des. 2015;87:721-731.

[28] Polmear IJ. Light Alloys - Metallurgy of the Light Metals. 3rd ed. London: Arnold; 1995, 112-114.

[29] Canaday CT, Moore MA, Tang W, Reynolds AP. Through thickness property variations in a thick plate AA7050 friction stir welded joint. Mater. Sci. Eng. A 2013;559:678-682.

[30] Brown R, Tang W, Reynolds AP. Multi-pass friction stir welding in alloy 7050-T7451: Effects on weld response variables and on weld properties. Mater. Sci. Eng. A 2009;513–514:115-121.

[31] Cerri E, Leo P. Mechanical properties evolution during post-welding-heat treatments of double-lap friction stir welded joints. Mater. Des. 2011;32:3465-3475.

[32] Li JQ, Liu HJ. Characteristics of the reverse dual-rotation friction stir welding conducted on 2219-T6 aluminum alloy. Mater. Des. 2013;45:148-154.

[33] Forcellese A, Simoncini M. Plastic flow behaviour and formability of friction stir welded joints in AZ31 thin sheets obtained using the 'pinless' tool configuration. Mater. Des. 2012;36:123–129.

[34] Kim D, Lee W, Kim J, Kim C, Chung K. Formability evaluation of friction stir welded 6111-T4 sheet with respect to joining material direction. Int. J. Mech. Sci. 2010;52:612–625.

[35] Rhodes CG, Mahoney MW, Bingel WH, Spurling RA, Bampton CC. Effects of friction stir welding on microstructure of 7075 aluminum. Scripta Mater. 1997;36:69-75.

[36] Reynolds AP. Visualization of material flow in autogenously friction stir welds. Sci. Technol. Weld. Join. 2000;5:120-124.

[37] Imam M, Biswas K, Racherla V. On use of weld zone temperatures for online monitoring of weld quality in friction stir welding of naturally aged aluminium alloys. Mater. Des. 2013;52:730-739.